Journal of Solid State Chemistry **153,** 106–117 (2000)
doi:10.1006/jssc.2000.8756, available online at http://www.idealibrary.com on IDEAL®

X-Ray Diffraction Studies of 2212-Type Superconductors in the Tl–Hg–Ba–Sr–Ca–Cu–O System

M. Valldor,*[,1] Ph. Boullay,*[,2] J. Axnäs,† and I. Bryntse*

*Department of Inorganic Chemistry, Arrhenius Laboratory, University of Stockholm, Stockholm SE-106 91, Sweden; and †Department of Solid State Physics, Royal Institute of Technology, Stockholm SE-100 44, Sweden

Received March 14, 2000; in revised form April 14, 2000; accepted April 20, 2000; published online July 7, 2000

Superconducting cuprates with the general stoichiometry $(Tl, Hg)_2(Ba, Sr)_2(Sr, Ca)_1Cu_2O_{8-\delta}$ were examined by X-ray powder diffraction, including Rietveld refinement calculations. The aim was to obtain structural properties that could be related to the diamagnetic transition onset temperature ($T_{c(onset)}$). R_w values for nine different samples, with different Ba, Sr, and Ca contents, were 0.105 or less. For three of the polycrystalline samples, the diamagnetic transitions were confirmed by resistivity measurements. Bond valence sum calculations indicate that $T_{c(onset)}$ increases (45–100 K) with a decreasing formal oxidation state of Cu in the superconducting plane. This tendency might be correlated with the apical distance between the (Ba, Sr) and Cu layers since the interplanar distance increases proportionally with the critical temperatures. In turn, this distance increases with the Ba/Sr ratio at the larger alkaline-earth metal site.

Key Words: **superconductor; X-ray powder diffraction; Rietveld refinement.**

INTRODUCTION

The copper oxide layers in superconducting cuprates are interesting because it is assumed that the superconductivity is confined within them. The hole doping is crucial for the transition temperature, but whether Cu^{3+} or O^{1-} is the charge medium is still under discussion (1). In the Hg–Ba–Ca–Cu–O system, the hole doping was changed by post annealing oxygenation by Marezio *et al.* (2) and an optimum was determined. Sun *et al.* (3) tried introducing Tl at the Hg site, which also probably affected the presence of oxygen and thereby the materials properties. Other substitutions at the Hg site within the charge reservoir layer were made by Isawa *et al.* (4), as Pb was introduced at this site. Re (5) and Cu (6) have also been reported as charge reservoir substitutents. The $(Tl, Hg)_2Ba_2Ca_1Cu_2O_{8-\delta}$ (2212) compound here in focus, with the atom ordering –$(Tl, Hg)O_x$–$(Tl, Hg)O_x$–BaO–CuO_2–Ca–CuO_2–BaO–, has been thoroughly investigated and subjected to several of the substitutions mentioned above. All of these different chemical modifications affect cell parameters, interatomic distances, and superconducting transition temperature. The superconducting Cu–O layer will likely be more affected by substitution at the alkaline–earth metal sites (Ba and Ca), which are the layers' closest structural neighbors. There are restrictions on the kinds of atoms that can be introduced at the larger (Ba) site, between $(Tl, Hg)O_x$ and CuO_2: Sr substitution has been examined by several groups and La by Subramanian *et al.* (7). However, the smaller (Ca) site, situated between the two adjacent Cu–O layers, has more substitutents: Sr (8)/Nd (8, 10)/Y (9)/Ce (10)/Dy (11)/Sm (12)/Pr (13). In some papers, Sr was reported to enter both alkaline-earth metal sites (14, 15), which makes this element special. All these substitutions affected structural properties, among which the apical Cu–O distance and the angles within the Cu–O layers have been found closely connected with the superconducting transition temperature, for instance by Ström *et al.* (16).

As reported earlier (17), almost phase-pure products with the general formula $(Tl, Hg)_2(Ba, Sr)_2(Sr, Ca)_1Cu_2O_{8-\delta}$ exhibit transition onset temperatures ($T_{c(onset)}$) ranging from 45 to 100 K, depending mainly on the ratios between Ba, Sr, and Ca. In the same paper it was shown that the cell parameters, a and c, increase proportionally with $T_{c(onset)}$. The reported compounds are resistant to oxidation and reduction up to 300°C. Here, the structural differences in the $(Tl, Hg)_2(Ba, Sr)_2(Sr, Ca)_1Cu_2O_{8-\delta}$ compounds will be investigated in detail and compared with the superconducting onset temperature, $T_{c(onset)}$.

A model of the investigated 2212 structure is presented in Fig. 1.

[1] To whom correspondence should be addressed. Fax: + 46-08-15 21 87. E-mail: beb@inorg.su.se.

[2] Laboratoire de Science des Procédés Céramiques et de Traitements de Surface (UMR6638), 123 Av. Albert Thomas, 87060 Limoges Cedex, France.

0022-4596/00 $35.00

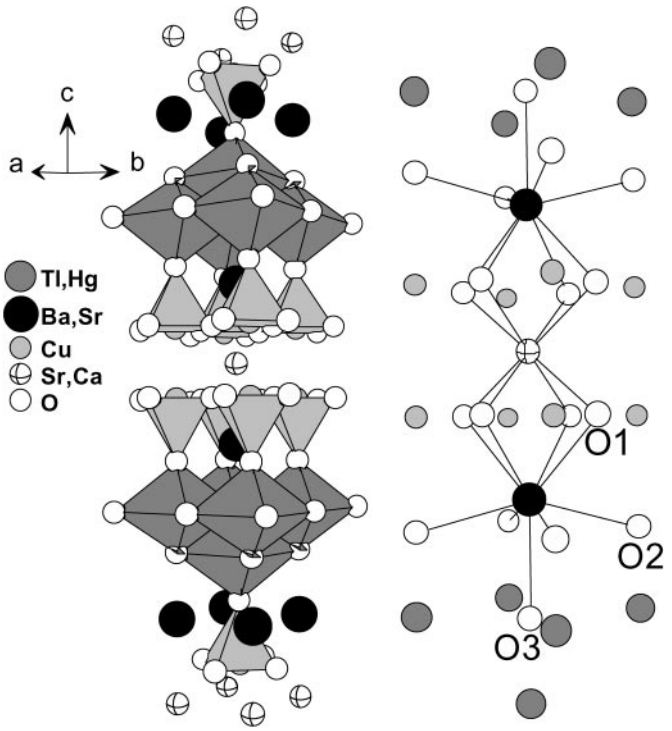

FIG. 1. Perspective view of the 2212 structure with polyhedra (left) centered on the Ca position. The ball-and-stick model (right) clarifies the coordinations at the two alkaline-earth metal sites: one eight-coordinated and two nine-coordinated sites. Crystal models were constructed with the Diamond Version 2.1c software.

EXPERIMENTAL

Synthesis and Elemental Analysis

The investigated materials were made, as described in detail elsewhere (14), from stoichiometric amounts of metal oxides in a powder reaction within closed vessels. Starting and resulting stoichiometries are presented in Table 1. In short, pure oxides were weighed and mixed in an agate mortar inside a glove box with an Ar atmosphere. The powder mixtures were pressed into pellets and placed in silica tubes, which were evacuated and completely sealed. All samples were then reacted using the same program, starting with a rise in temperature up to 880°C for 5 h. This temperature was held for 5 h, followed by a controlled cooling, of about 1°/min, down to 400°C. Further cooling down to room temperature continued inside the furnace. Empirically, it has been shown that a slow cooling rate from 880°C to 400°C causes less strain on the tube walls and decreases the risk of tube damage.

The resulting stoichiometries were determined by energy-dispersive spectrometry (EDS) analyses with corrections for atomic number, absorption, and fluorescence (ZAF), using the Si detector LINK AN10000 attached to a JEOL 820 scanning electron microscope (SEM) with 20 kV of accelerating voltage. Two samples with intermediate composition were also examined in a JEOL 2000FX transmission electron microscope (TEM) at 200 kV of accelerating voltage. EDS analyses on the diffracting crystals, using a connected LINK AN10000, confirmed the previously established compositions.

Resistivity Measurements

In the resistivity measurements a four-probe method was used, where a direct current (dc) was led through a polycrystalline pellet at the same time the electrical potential (V) was measured at two positions, in between the current contacts, in the same direction as the current flow. To increase the contact to the pellets, the contact areas were sputtered with gold onto which gold wires were fastened, using silver paint (Degussa AG D200). The sputtered areas were separated by Al-foil coverage. No heat treatment was necessary for the

TABLE 1
Elemental Analyses of Crystals within the Polycrystalline Samples

Start stoichiometry	$T_{c(onset)}$	EDS result
$Tl_{1.5}Hg_{0.5}Ba_2Ca_1Cu_2O_{8-\delta}$	100 K	$Tl_{1.54}Hg_{0.54}Ba_{1.88}Ca_{0.96}Cu_{2.1}O_{8-\delta}$[a]
$Tl_{1.3}Hg_{0.7}Ba_{1.5}Sr_{0.75}Ca_{0.75}Cu_2O_{8-\delta}$	97 K	$Tl_{1.40(6)}Hg_{0.55(4)}Ba_{1.4(1)}Sr_{0.8(1)}Ca_{0.57(7)}Cu_{2.3(1)}O_{8-\delta}$[b]
$Tl_{1.3}Hg_{0.7}Ba_{1.75}Sr_{0.75}Ca_{0.5}Cu_2O_{8-\delta}$	94 K	$Tl_{1.33(4)}Hg_{0.61(4)}Ba_{1.53(8)}Sr_{0.8(1)}Ca_{0.5(1)}Cu_{2.3(1)}O_{8-\delta}$[b]
$Tl_{1.3}Hg_{0.7}Ba_{1.5}Sr_{1.25}Ca_{0.25}Cu_2O_{8-\delta}$	91 K	$Tl_{1.28(5)}Hg_{0.61(3)}Ba_{1.4(1)}Sr_{1.1(1)}Ca_{0.7(3)}Cu_{2.41(7)}O_{8-\delta}$[b]
$Tl_{1.3}Hg_{0.7}Ba_{1.5}Sr_1Ca_{0.5}Cu_2O_{8-\delta}$	89K	$Tl_{1.30(5)}Hg_{0.60(4)}Ba_{1.3(1)}Sr_{1.1(2)}Ca_{0.4(1)}Cu_{2.4(1)}O_{8-\delta}$[b]
$Tl_{1.3}Hg_{0.7}Ba_{1.75}Sr_{0.5}Ca_{0.75}Cu_2O_{8-\delta}$	86 K	$Tl_{1.37(7)}Hg_{0.56(4)}Ba_{1.62(9)}Sr_{0.46(9)}Ca_{0.85(4)}Cu_{2.1(1)}O_{8-\delta}$[b]
$Tl_{1.3}Hg_{0.7}Ba_1Sr_{1.25}Ca_{0.75}Cu_2O_{8-\delta}$	80 K	$Tl_{1.390(6)}Hg_{0.58(6)}Ba_{1.06(8)}Sr_{1.15(8)}Ca_{0.60(4)}Cu_{2.2(1)}O_{8-\delta}$[b]
$Tl_{1.3}Hg_{0.7}Ba_{0.6}Sr_{1.8}Ca_{0.6}Cu_2O_{8-\delta}$	60 K	$Tl_{1.39(6)}Hg_{0.60(4)}Ba_{0.6(1)}Sr_{1.5(2)}Ca_{0.7(1)}Cu_{2.2(2)}O_{8-\delta}$[b]
$Tl_{1.3}Hg_{0.7}Ba_{0.8}Sr_{1.4}Ca_{0.8}Cu_2O_{8-\delta}$	55 K	$Tl_{1.37(6)}Hg_{0.588(4)}Ba_{0.71(8)}Sr_{1.3(1)}Ca_{0.87(9)}Cu_{2.2(2)}O_{8-\delta}$[b]
$Tl_{1.3}Hg_{0.7}Sr_2Ca_1Cu_2O_{8-\delta}$	45 K	$Tl_{0.8}Hg_{0.7}Sr_{1.9}Ca_{1.1}Cu_{2.5}O_{8-\delta}$[c]

Note. The standard Deviations are calculated from 15–20 analyses per sample.
[a]Ref. (19).
[b]Ref. (17).
[c]Ref. (14).

Ag paint to solidify, which helped to avoid contamination of the sample or possible amalgamation between Au/Ag and Hg. The resistance between the contact and the sample was typically 10 Ω or less. To eliminate any risk of reactions between the Ag and the pellet during the measurements or the presence of thermopower effects, two opposite current directions were used for each data point.

The current in the resistivity measurements, 1 mA or less, was generated with a Keithley 2400 sourcemeter, and the voltage drop was observed with a Hewlett-Packard 3458A multimeter. The temperature was determined with a standard platinum sensor. A LakeShore 340 temperature controller was used to sweep the temperature slowly (1°/min) across the superconducting transition.

X-Ray Powder Diffraction

X-ray powder diffraction patterns for Rietveld refinements were obtained with a STOE STADI\P diffractometer in symmetric transmission mode, using a Ge monochromator to define the Cu$K\alpha$ radiation ($\lambda = 1.5405$ Å). Data were collected from 5° to 130° (2θ) in steps of 0.2°, at 40 kV and 50 mA, with an exposure time of 350 s for each step. Rietveld refinement calculations were accomplished with the Fullprof98 (18) software package. Nine different samples with the general stoichiometry $(Tl, Hg)_2(Ba, Sr)_2(Sr, Ca)_1Cu_2O_{8-\delta}$ (Tl/Hg ratio ~ 3) were included in the present investigation. The sample compositions and structural properties are presented in Table 2.

The background was set manually for all the refinements. The same starting values for fractional coordinates of all atoms, taken from recent results (14), were used throughout the data series. Thermal displacements parameters (β) for all atoms were initially set at 1.0 Å^2. Due to similar X-ray scattering factors, Tl and Hg were represented together as Tl. The relative occupancies of Ba, Sr, and Ca were set equal to values calculated from the EDS results in Table 1, which have been reported previously (17). Ba was placed only at the larger of the two alkaline-earth metal sites, and Ca was assumed to be present only at the smaller site. Sr was distributed to complete both sites, on the assumption that neither site is deficient. The minor excess of Cu was not accounted for.

Starting values for the cell parameters were taken from previously reported values (17) and were refined together with the zero position and total scaling factor as the first parameters, placing the Bragg positions fairly close to their optima. The shapes of the peaks were represented by a pseudo-Voigt function (No: 5); its weighting and shape parameters were carefully refined, at first separately but finally together with the cell parameters and zero position. Two asymmetry parameters were also refined with an angular limit set to $2\theta = 50°$.

Fractional coordinates were refined one by one and, after individual convergence, as a whole. With highly anisotropic crystal shapes, an alignment effect was expected in the [001] direction. Temporarily locking all parameters except the scaling factor, the Gaussian-preferred orientation distribution was refined in this direction. After convergence was reached again, with all parameters mentioned above, everything was fixed and the thermal displacements of individual metal positions were tried as least-squares parameters. All oxygen atoms were refined with a common thermal displacement parameter.

Since the data were obtained by X-ray diffraction in transmission mode, absorption effects make the thermal displacement less reliable, especially for lighter elements such as oxygen and perhaps calcium. In cases where absorption was obvious, as indicated by abnormal β values for any of the lighter elements, the thermal displacement was set to 1.0 for oxygen and in some cases also for the calcium-containing site. The standard deviations of the thermal displacement parameters could be obtained by using a full damping factor (computed shift = 0) for these sites during the refinements. As the O3 site (see Fig. 1), situated inside the charge reservoir layers often contains vacancies (δ), the occupancy at this site was added as the last parameter.

In additional investigations of the previously known Sr-free 2212, $Tl_{1.5}Hg_{0.5}Ba_2Ca_1Cu_2O_{8-\delta}$ (19), O3 was also displaced from the 00z position to x0z to further account for the high anisotropy at this site.

In nearly all samples, traces of some additional phase were present, but probably not more than 5% as judged from the X-ray intensities, indicated either by visible peaks or an unacceptable total curve fit, i.e., $\chi^2 > 3$. The impurity phases were identified by EDS and characteristic XRD peaks to be small amounts of either the lower homologue 2201 (20), Ca_2CuO_3 (21), Ba_2CuO_3 (22), or $BaCuO_2$ (23). The impurities found in the samples, added to the refinements, are listed in Table 2.

As 2212 and 2201 have similar a parameters, many reflections, e.g., the dominant 110 peak, appear at almost the same 2θ. This may add difficulties with intensities during the structural refinements. The scaling factor and cell parameters were in some cases refined for the impurities. The peak shapes for all additional phases were the same as those for the main phases within the host sample. In total, 23–25 parameters covered each of the Rietveld calculations discussed above. There were 154–160 observed reflections in the nonexcluded regions, giving more than 6 times as many reflections as parameters, which should be statistically tolerable.

Bond Valence Sum Calculations

The bond valence sum (BVS) calculations were executed as described by Brown and Altermatt (24). Comparing

TABLE 2
Structure Parameters for All Rietveld-Refined Compounds

$T_{c(onset)}$	45	55	60	80	86	89	91	94	97	100
Sr/Ca (occ.)	26/74	9/91	28/72	40/60	10/90	57/43	72/28	47/53	43/57	0/100
2*a* (0, 0, 0)										
β (Å^2)	0.79(8)	1.0(2)[a]	1.0(1)[a]	0.23(8)	0.2(1)	1.7(1)	1.9(2)	1.2(1)	1.0(1)	0.2(1)
Ba/Sr (occ.)	85(Sr)/15(Ca)	37/63	32/68	53/47	83/17	70/30	75/25	81/19	70/30	100/0
4*e* (0, 0, *z*)	0.12126(6)	0.1209(1)	0.1217(1)	0.12218(6)	0.12179(7)	0.12230(8)	0.1232(1)	0.12245(9)	0.12175(8)	0.12183(5)
β (Å^2)	0.95(6)	3.08(8)	2.03(8)	1.07(4)	1.34(5)	1.54(6)	1.69(9)	1.34(7)	1.59(6)	1.92(4)
Tl/Cu (occ.)	75/25	100/0	100/0	100/0	100/0	100/0	100/0	100/0	100/0	100/0
4*e* ($\frac{1}{2}$, $\frac{1}{2}$, *z*)	0.21226(3)	0.21192(6)	0.21219(7)	0.21262(4)	0.21264(5)	0.21270(6)	0.21325(9)	0.21303(7)	0.21254(6)	0.21260(5)
β (Å^2)	0.81(2)	2.25(3)	2.23(4)	1.39(2)	1.27(3)	1.39(3)	1.25(4)	1.45(4)	1.77(3)	2.43(3)
Cu (occ.)	100	100	100	100	100	100	100	100	100	100
4*e* ($\frac{1}{2}$, $\frac{1}{2}$, *z*)	0.05794(8)	0.0572(1)	0.0586(2)	0.0576(1)	0.0565(1)	0.0575(1)	0.0591(2)	0.0572(2)	0.0565(1)	0.0545(1)
β (Å^2)	0.14(5)	0.72(9)	1.0(1)	1.40(8)	0.26(9)	0.3(1)	0.3(2)	1.4(1)	0.25(9)	0.97(8)
O1 (occ.)	100	100	100	100	100	100	100	100	100	100
8*g* (0, $\frac{1}{2}$, *z*)	0.05580(4)	0.0540(4)	0.0536(6)	0.0555(3)	0.0539(4)	0.0553(5)	0.0564(6)	0.0538(5)	0.0558(4)	0.0525(3)
β (Å^2)	2.1(2)	1.0(2)[a]	2.4(3)	1.1(1)	2.0(2)	2.1(2)	2.1(3)	1.0(2)[a]	1.0(2)	1.2(2)
O2 (occ.)	100	100	100	100	100	100	100	100	100	100
4*e* ($\frac{1}{2}$, $\frac{1}{2}$, *z*)	0.1404(6)	0.1429(7)	0.136(1)	0.1415(6)	0.1407(8)	0.1391(8)	0.144(1)	0.1395(8)	0.1426(8)	0.1441(5)
β (Å^2)	2.8(2)	1.0(2)[a]	2.4(3)	1.1(1)	2.0(2)	2.1(2)	2.1(3)	1.0(2)[a]	1.0(2)	1.2(2)
O3 (occ.)	75(5)	95(3)	100(4)	75(2)	70(3)	71(3)	77(5)	72(4)	47(3)	90(4)
16*n* (*y*, $\frac{1}{2}$, *z*)										0.148(6)
4*e* ($\frac{1}{2}$, $\frac{1}{2}$, *z*)	0.2148(7)	0.2134(8)	0.2246(9)	0.2168(9)	0.219(1)	0.224(1)	0.230(1)	0.224(1)	0.219(2)	0.2223(8)
β (Å^2)	2.7(5)	1.0(2)[a]	2.4(3)	1.1(1)	2.0(2)	2.1(2)	2.1(3)	1.0(2)[a]	1.0(2)	1.2(2)
a (Å)	3.796(3)	3.81766(1)	3.81884(5)	3.83149(1)	3.84372(1)	3.84860(3)	3.86031(1)	3.85299(1)	3.84456(1)	3.84781(0)
c (Å)	28.433(2)	28.9110(1)	28.8665(6)	29.12254(6)	29.38761(7)	29.4179(3)	29.6022(1)	29.4878(1)	29.32876(9)	29.51044(4)
Std. multp.		3.1066	3.9515	2.5731	3.0308	3.2664	3.6026	4.0955	2.7625	2.8488
R_W	0.025	0.114	0.0902	0.0653	0.0822	0.0785	0.100	0.0877	0.0771	0.0701
R_F	—	0.0914	0.0888	0.0743	0.079	0.078	0.0852	0.0865	0.0797	0.0524
R_{Bragg}	—	0.0958	0.104	0.0691	0.0837	0.0847	0.0998	0.0981	0.0979	0.0501
χ^2	—	1.55	1.79	1.18	1.70	1.86	2.83	2.18	1.65	2.38
hkl	181	155	154	156	157	158	160	159	157	158
Param.	30	23	23	23	24	23	25	25	23	24
Imp. or	—	—	2201	27.18–28.94	$BaCuO_2$	Ba_2CuO_3	2201	2201	29.43–30.26	$BaCuO_2$
Excl. reg.[b]			Ba_2CuO_3	35.45–35.67		Ca_2CuO_3		$BaCuO_2$	36.98–37.49	
(2θ)				38.53–38.9					38.39–39.26	
Fig.		3a	3b	3c	3d	3e	3f	3g	3h	3i

Note. The compositions corresponding to the T_c-values are presented in Table 1.
[a] Indicate β values, which were manually set to 1.0, as explained in the text.
[b] Impurity phases or excluded regions added to the Rietveld refinement.

empirical tabulated values of bond distances (24) with measured bond distances for a certain pair of atoms yields a valence distribution of that particular bond. If the valence contributions of all neighboring atoms are added together, the sum will be an approximate oxidation state of the central atom. For starters, oxidation states of the interacting atoms have to be assumed, from which the result is allowed to deviate. Note that BVS calculations apply to unstrained crystals; however, the results could well be used for comparisons between the samples examined below. All bond valence sum calculations were performed with the VALENCE (25) software program.

RESULTS AND DISCUSSION

Resistivity Measurements and Electron Microscopy

The curves presented in Fig. 2 are normalized to the resistance at 150 K. Comparing the resistance curves with

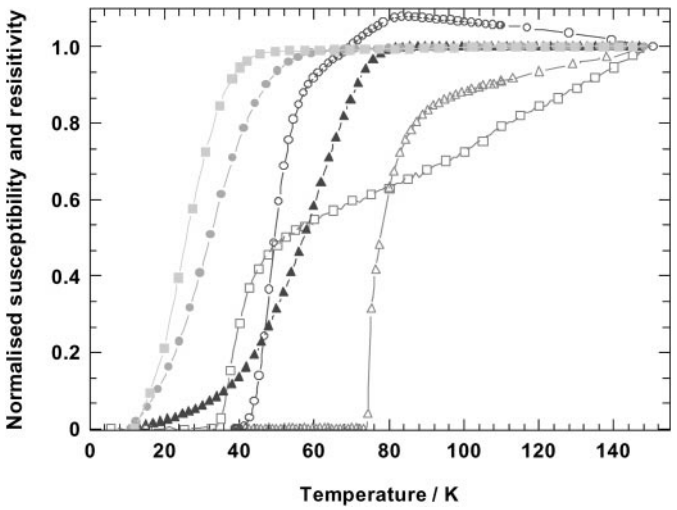

FIG. 2. T_c measurements, susceptibility (filled markers), and resistivity (empty markers) for three samples. The normalization start from 150 K. The samples included are $T_{c(onset)} = 80$ K (triangles), $T_{c(onset)} = 55$ K (circles), and $T_{c(onset)} = 45$ K (squares).

previously measured susceptibility measurements also normalised for the sake of comparison, it is possible to see an agreement between zero-resistance temperature and the diamagnetic transition (T_c). All samples became superconducting since zero resistivity was reached. Ideally, the resistivity disappears at a certain temperature. However, several factors may broaden the transition. As the pellets are polycrystalline, the conductivity is somewhat limited by the character of the grain boundaries. The resistivity for one sample increased slightly up to 85 K, after which a metallic behavior dominated down to the superconducting transition. The increase in resistivity could be explained in terms of quantum interference effects since the room temperature resistivity was very high, well above 1×10^{-4} Ωm. Also, for this sample the contacts were not prepared on freshly cut surfaces and aging of the sample surface may have influenced the results. For the samples containing more than one mixed site, inhomogeneities could contribute to a broadening of the resistivity drop. Apart from different metal ratios at the mixed sites, the oxygen stoichiometry might vary within a sample.

A few of the intermediate stoichiometries were examined by transmission electron microscopy. Electron diffraction helped exclude the possibility of having superstructures. Only weak streaking was detected along the c^* axis, indicating possible disorder (stacking faults), but the dominating part of the crystals agreed well with the 2212 structure. As could be seen in Table 1, all the resulting compositions, achieved by EDS in the SEM, are fairly similar regarding Tl, Hg, and Cu. The slight excess of Cu could possibly have entered the (Tl, Hg) site, as has been discussed in several Hg-containing systems (6,14).

Rietveld Refinements

For all samples, the calculations were performed in the space group *I*4/*mmm*. Observed and calculated diffraction patterns for all compositions together with their intensity differences are presented in Figs. 3a–3i. When previously refined cell parameters, obtained from Guinier–Hägg X-ray powder data (17), are compared with the ones obtained from the Rietveld calculations presented above, it is obvious that they agree well. Moreover, they appear to be correlated with $T_{c(onset)}$ (Fig. 4) since samples with longer unit cell axes give higher values of $T_{c(onset)}$. In a system having three mixed sites (Tl,Hg, Ba,Sr, Sr,Ca) and a partially occupied position (O3), there is an obvious possibility of solid solutions. Asymmetric intensities or broadening of singly indexed peaks at high angles could indicate solid solution, i.e., varying cell parameters. However, the peaks were visually symmetrical at the same time the peak asymmetry parameters showed reasonable values, indicating well-defined phase compositions within the samples.

Results for intermediate compositions, containing Sr at both alkaline-earth metal sites, were expected to be less accurate than those for the end compositions, $Tl_{0.8}Hg_{0.7}Sr_2Ca_1Cu_{2.5}O_{8-\delta}$ and $Tl_{1.5}Hg_{0.5}Ba_2Ca_1Cu_2O_{8-\delta}$, since there are two more mixed sites apart from the Tl,Hg site (Ba,Sr, Sr,Ca). Finally, all R_w values were below 0.105, and R_F ended up at 0.09 or less. R_{Bragg} was fairly similar to R_F or just above it (see Table 2). The R values for the compound without Ba were better by far than the others since it originates from a single-crystal refinement published in previous work (14).

R_{Bragg} is affected by the intensity differences at the Bragg positions, which in these refinements were due to the 107 and 110 peaks. Refining the preferred orientation had little effect on the R_{Bragg} value, but a slight manual shift in the absorption correction (μR), without introducing an abnormal value, made some displacement factors (β) more tolerable (< 3.0 Å^2), also lowering R_{Bragg} somewhat. The common problem regarding thermal displacement and occupancy of O3, discussed by several other investigating groups, originates from the fact that the X-ray scattering from a light atom situated between heavy atoms is difficult to quantify. The thermal displacement probability ellipsoids of Tl and O3 will overlap to some extent.

As for the data obtained, a few of the XRPD patterns show an abnormal background in the 15–25° 2θ range, due to the amorphous glue used for making the powder stick to the sample holder. The most important reason for the bump only being present in some XRPD patterns was the differences in intensities. The polynomial function in the Rietveld refinement program did not succeed in adjusting to this bump. To avoid introduction of additional parameters to differentiate between the samples, all data sets were treated with a manually set background, and it was assumed that

the results comparisons were not affected by this treatment. The differences in total intensity between the measurements were likely due to absorption, which could be explained in several ways. The most prominent factors for absorption were the presence of heavy atoms (Hg and Tl) and the difficulties in achieving small crystal sizes. Thorough grinding of the polycrystalline sample might decrease the average crystal size below 10 μm. Small changes in the average crystal size and the amount of sample were therefore reasons for noticeable absorption in a few of the diffractograms.

Investigated Distances

To find any structure–$T_{c(onset)}$ correlation, many distances were checked against $T_{c(onset)}$, based on the results from Table 2. The in-plane distance between Cu and O1 increased with $T_{c(onset)}$ (Fig. 5a) in a way fairly similar to that of the *a* cell parameter. This tendency is expected because the superconducting Cu–O layer is almost flat in all cases. Small deviations from the planar configuration are plotted as the difference between the Cu and the O1 *z* coordinates (Fig. 5b). The puckering of the Cu–O layer does not seem to correlate with $T_{c(onset)}$, but the accuracy of the data has to be more reliable (smaller STD) to exclude such a correlation. At the same time as Cu moves away from the O1 plane, it should come closer to the apical oxygen (O2). However, the apical distances show no obvious connection to the in-plane puckering, but instead increase with $T_{c(onset)}$ (Fig. 5c). The larger alkaline-earth metal site, containing different Ba/Sr ratios, may also be examined regarding the bond lengths. As the determination of the oxygen sites will include high standard deviations, depending on oxygen's low X-ray

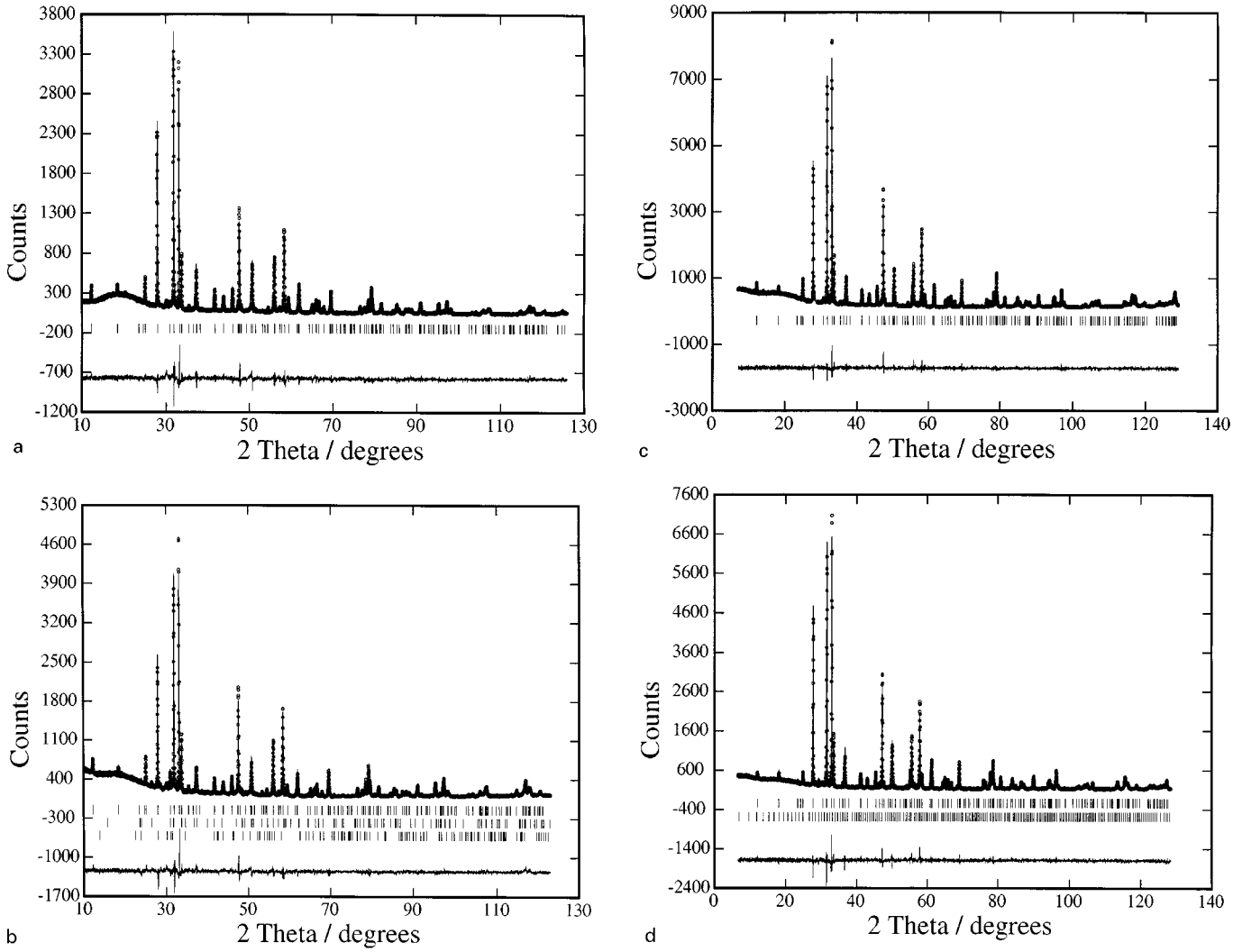

FIG. 3. (a–i) Powder X-ray diffraction patterns of all Rietveld-refined compounds. Calculated intensities are indicated with circles and measured diffraction patterns and the intensity differences are represented by solid lines. Vertical bars indicate the Bragg positions for the main phase (upper) and the impurities (below).

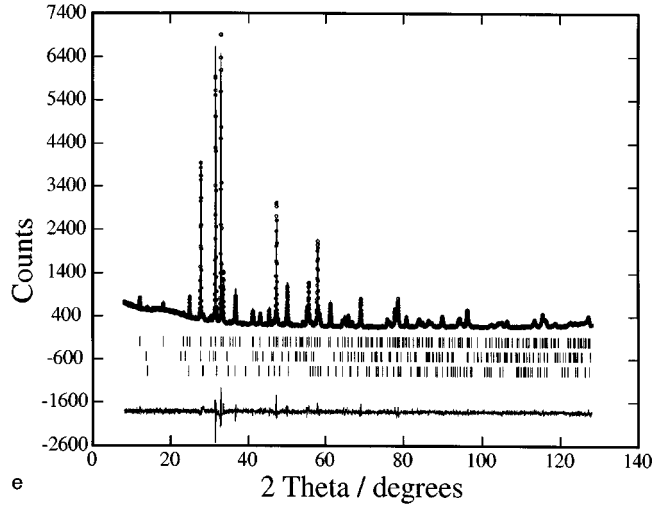

e

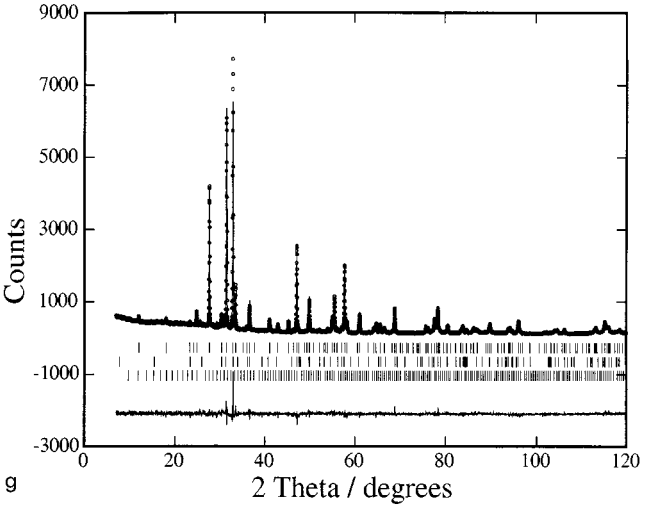

g

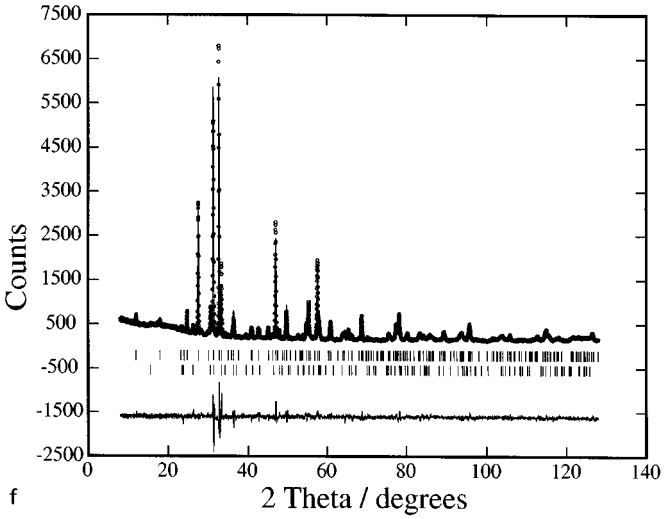

f

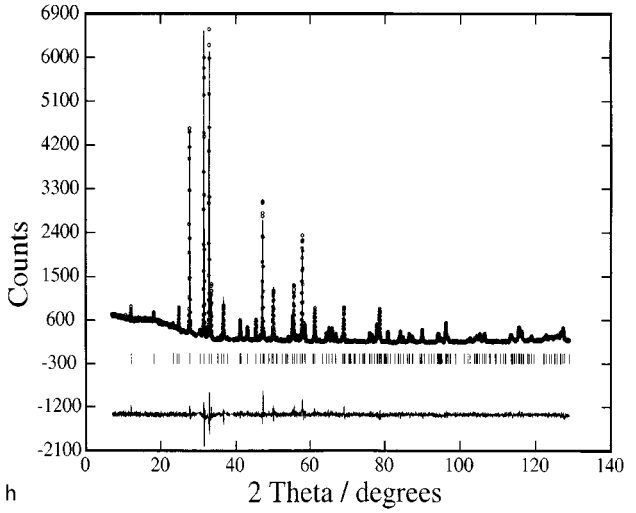

h

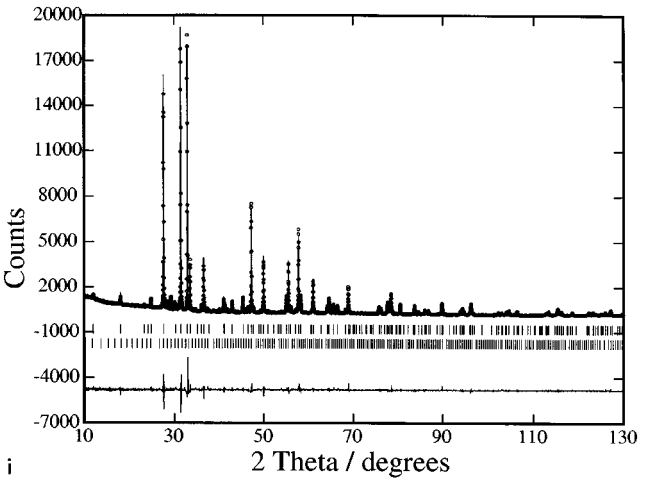

i

FIGURE 3—*Continued*

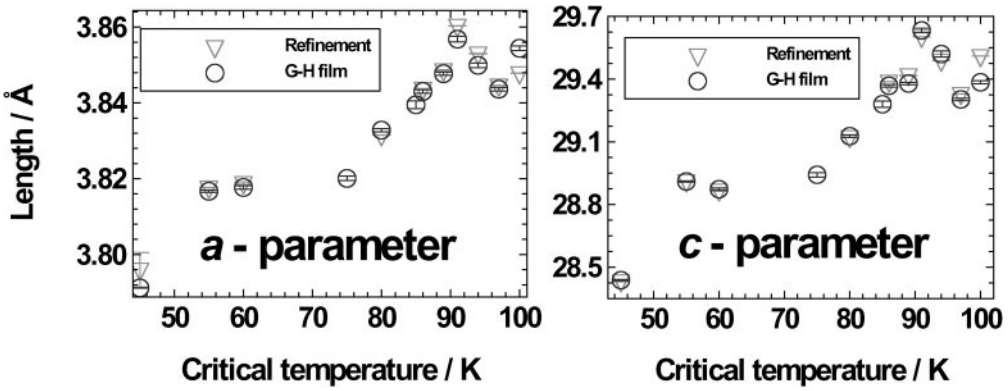

FIG. 4. A comparison between cell parameters obtained with a Guinier–Hägg camera using an internal Si standard (G–H film, circles, previously published (17)) and the results from Rietveld refinements (refinement, triangles). One STD and the Bérar–Lelann factor are included in the Rietveld-refined results (3 STD for G–H data) for all samples except the single-crystal refinement (at 45 K), which has 3 STD.

scattering, a comparison between the (Ba,Sr) plane (z coordinate) and the Cu plane (z coordinate) should be more accurate. It seems that the distance between the metal planes changes with $T_{c(onset)}$ (Fig. 5d). Moreover, the movement of the (Ba,Sr) site upward, away from the Cu–O layer, is most likely induced by a change in the Ba/Sr ratio at this site. As seen in Fig. 5e, the distance between the layers is correlated to the Ba content.

According to Bérar and Lelann (26), STDs from Rietveld refinements can be decreased using higher resolution, in this case a shorter analyzing step in 2θ when obtaining XRPD data. Below a certain limit of resolution, the resulting data will give no additional structural information, even though the STDs will still decrease, and the results are therefore probably too optimistic. A multiplication factor has been suggested, giving larger but more reliable deviations. These factors are presented in Table 2 as "Std.Multp." affecting all standard deviations equally within the same calculation, but they have not been accounted for in Table 2. However, presented standard deviations have already been rounded off upward and therefore have slightly higher values than those expected when multiplied as tabulated. In all of the plotted structural properties vs $T_{c(onset)}$ (Figs. 5a–5e) the Bérar–Lelann factor has been included. Note that such factors are normally not included in other various reports.

Bond Valence Sums

As the BVS is calculated for Cu in all intermediate compositions (Fig. 6a), four bonds between Cu and O1 in addition to one bond between Cu and O2 are included. The latter contributes insignificantly to the valence, but is probably very important for the charge distribution between the charge reservoir and the superconducting planes. The Cu–O1 distances are closely connected with the a cell parameter (Cu–O1 $\sim a/2$) because the Cu–O layers are almost flat. However, the Cu–O2 bond is more dependent on the size of the ions situated within the charge reservoir and at the (Ba,Sr) site. The comparison between BVS for Cu and $T_{c(onset)}$ indicates that the oxidation state of Cu decreases with increasing critical temperature, except for one sample ($T_{c(onset)} = 60$ K), which deviates slightly. Note that the inclusion of the bond between Cu and O2 almost doubled the standard deviations because this bond length is not symmetry-restricted like the Cu–O1 bond, where the dominating part of the distance is determined by the fractional coordinates $x = y = 1/2$ (Cu) and $x = 0(1/2)$, $y = 1/2(0)$ (O1). The sample with the highest $T_{c(onset)}$ has a BVS(Cu) of 2.13(2), which corresponds to $\delta = 0.24$ in $Tl_{1.5}Hg_{0.5}Ba_2Ca_1Cu_2O_{8-\delta}$, assuming all other elements to have their nominal oxidation state.

When the Ba content was compared with the BVS of Cu, it was clear that a higher content of Ba lowered the Cu valence (Fig. 6b), which is the expected tendency since the Cu–O bond distances are extended with a larger ion at the nine-coordinated site. Because the calculated oxidation state of Cu in the (Tl,Hg)-2212 phases decreases with increasing atom size at the (Ba,Sr) site, less oxygen should be present in the charge reservoir at the same time. By simple reasoning, it could be argued that a larger atom at the (Ba,Sr) site would occupy a part of the space belonging to O3 and therefore suppress the occupancy of O3. To understand this, one should examine the (Ba,Sr) site, which is nine-coordinated (monocapped square antiprism) (see Fig. 1). The metal atom is displaced from the center of the square antiprism toward the capping, situated close to the layer of the four oxygens on the capped side. An expansion of the upper square is therefore expected. With larger ions, the metal site should shift toward the capping, almost reaching the expanded oxygen plane (O2), moving closer to the charge reservoir layer oxygen (O3), displacing it or affecting its occupancy.

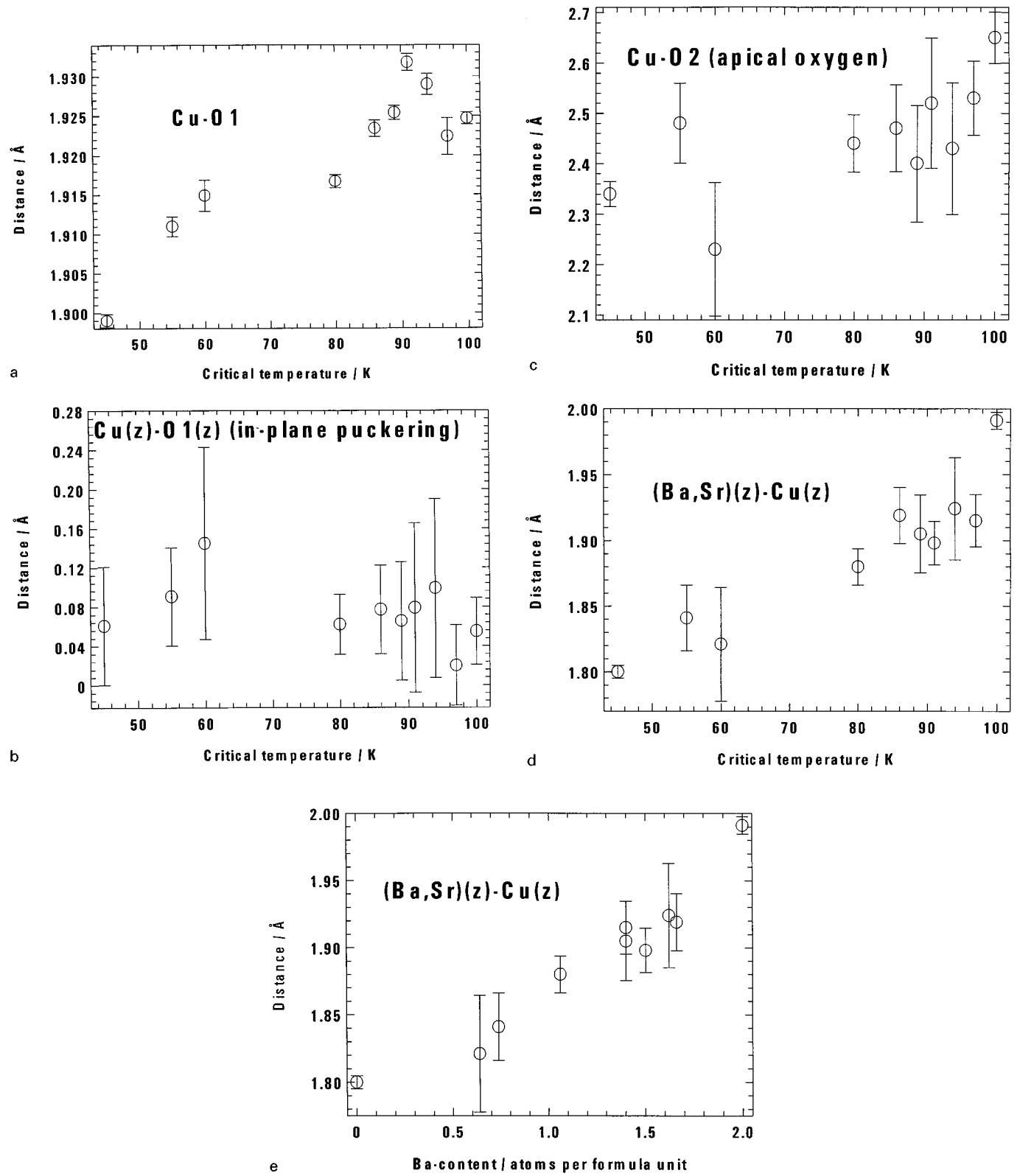

FIG. 5. (a–e). For all diagrams, 1 STD is included, multiplied by the factor suggested by Bérar and Lelann (between 2.6 and 4.4). The sample farthest to the left in all graphs (single-crystal refinement) is presented with 3 STD.

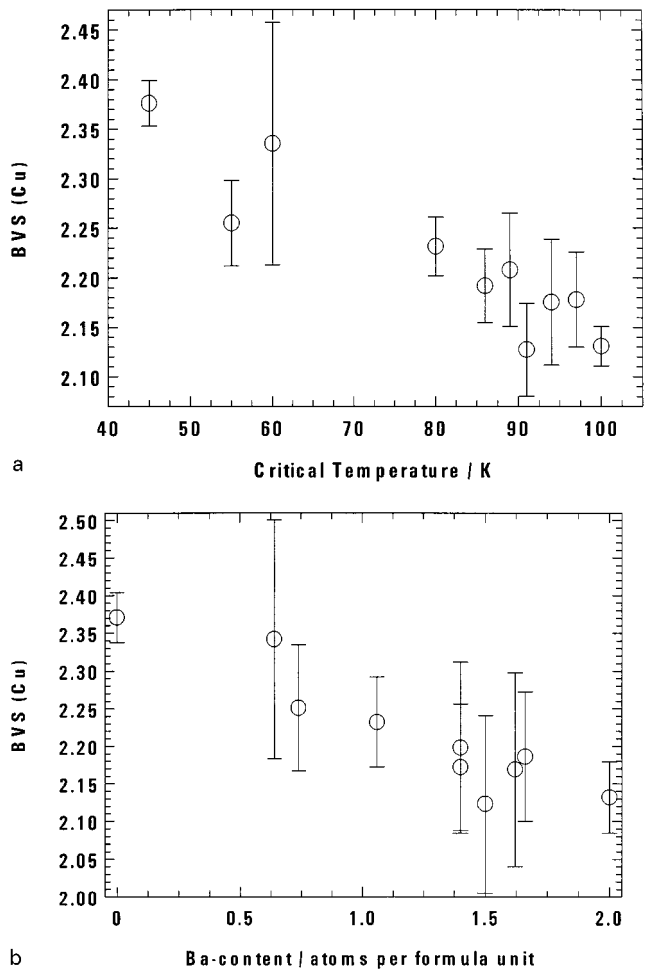

FIG. 6. (a, b). BVS for Cu vs T_c (a) and Ba content (b). One STD, multiplied by the factor suggested by Bérar and Lelann, is included. The sample farthest to the left in all graphs (single-crystal refinement) is presented with 3 STD.

Commenting on whether Cu or O is responsible for the hole concentration, it is interesting that no correlation between $T_{c(onset)}$ and the Cu–O(apical) distance was found (Fig. 5c), whereas the Cu valence had some connection with $T_{c(onset)}$ (Fig. 6a). This could prove that the in-plane bond affects the hole doping to a higher degree than does the apical bond. Thus, the superconducting holes could be situated on oxygen, indicating O^{1-}/Cu^{2+} as suggested by Nücker *et al.* (1) and others, rather than O^{2-}/Cu^{3+}, because the latter charge distribution introduces a higher difference in chemical potential. For simplification, when hole doping in the superconducting planes is being discussed, the holes are assumed to belong to Cu, even though Nücker *et al.* (1) argued that the density of states with energies closest to the Fermi level belongs to O 2*p* instead of Cu 3*d*. If the holes were placed on the oxygen, giving O^{1-}, then the O1–Cu bond would give the dominant part of the oxygen valence, while contributions from the (Sr,Ca) sites should be less significant. High-resolution electron-energy loss spectrometry (HREELS) reported by Romberg *et al.* (27) indicates that the oxygen $2p_{xy}$ orbitals contain the holes in the $Tl_2Ba_2Ca_1Cu_2O_8$ compound.

Comparisons

An investigation of the effect of the ionic radius changes in cuprates has been previously reported by Attfield *et al.* (28). In this report the critical temperature of La_2CuO_4 (LCO) was altered with the substitution of La for different ions having the same or a lower oxidation state. La, Nd, Ba, Sr, and Ca were randomly placed at the "La site". Three series of compounds were presented and an optimum mean radius was found. Applying the same idea here to the Ba,Sr,Ca-2212 system gives similar results since the critical temperature is dependent on the mean size of alkaline-earth metal atoms at the two possible sites in the 2212 structure. However, instead of finding an optimum, $T_{c(onset)}$ increased with the atomic size at the larger of the alkaline-earth metal sites, without reaching a maximum. For Sr-free 2212 the critical temperature was about 100 K, and to reach a higher value by substitution may require an ion larger than Ba^{2+}, having the same oxidation state.

The fact that the largest ion at the nine-coordinated site gives the highest critical temperature contradicts the experimental increase in T_c with pressure reported by Chu *et al.* (29) for the Hg-1223 superconductor, where an increase in pressure shortened the bond lengths within the Cu–O layers, whereas Ba, in the results presented here, expands the crystal unit cell and therefore increases the in-plane bond lengths. It is likely that the applied pressure resulted in structural changes that could not be induced by chemical means in our study.

Ström *et al.* (16) have proposed that the inclusion of Sr at the Ba site, in the closely related $Tl_2Ba_2Ca_1Cu_2O_8$, will not affect T_c significantly up to a doping level of 30% ($Ba_{1.4}Sr_{0.6}$), even though the (Ba,Sr) site moves with different Ba/Sr ratios. It was stated that the (Ba,Sr) site comes closer to the plane of the apical oxygen with increasing Sr content, at the same time as both Tl and Cu approach the apical oxygen in the *z* direction. With Cu moving upward, the puckering of the Cu–O layers increased, but does not result in an expected rapid decrement in $T_{c(onset)}$. The results of (Tl,Hg)-2212, presented here, did not exhibit the same tendencies with Sr content, but instead exhibited a large variety of critical temperatures. There are explanations for this, one of which could be the fact that Sr has entered both sites in the present investigation. Or it is not possible to ignore that Hg, with its lower oxidation state compared to that of Tl, gives more opportunities for oxygen content and hole concentration to vary.

Concerning the BVS–$T_{c(onset)}$ comparison, Maignan *et al.* (30) reported that $Tl_{1.5}Hg_{0.4}Sr_{2.2}Ca_{0.8}Cu_2O_{8-\delta}$ became

superconducting at 25 K. However, BVS calculations on reported bond lengths gave an oxidation state of 2.31(2) for Cu, which is relatively high but still lower than 2.38(2), as for the earlier investigated $Tl_{0.8}Hg_{0.7}Sr_2Ca_1Cu_{2.5}O_{8-\delta}$ $T_{c(onset)} = 45$ K(14). This could be explained by the higher concentration of Tl in their 25 K compound, moving charge from the Cu-O layer to the charge reservoir layers provided that the presence of oxygen is fairly similar in both cases. If the Tl content in the 25 K case would have been the same as that in the 45 K phase, the Cu valence should have been higher because the apical oxygen moves away from the charge reservoir and approaches Cu, increasing the valence above 2.38, which would make the 25 K compound fit into the comparison.

Moreover, Ohta *et al.* (9) investigated the structure of $(Tl_{0.7}Hg_{0.3})_2Ba_2Y_{0.8}Ca_{0.2}Cu_2O_{8+\delta}$ and calculated BVS for Cu to be 2.084, and they also presented the results from iodometric titration, indicating that Cu should have an oxidation state of $+2.14(1)$. The authors claim that the phase is underdoped with hole carriers and reported a transition temperature of 65 K. Adding this phase to the BVS–$T_{c(onset)}$ comparison indicates that the optimum hole concentration has been surpassed since T_c has decreased compared with that of the $Tl_{1.5}Hg_{0.5}Ba_2Ca_1Cu_2O_{8-\delta}$ compound (BVS = 2.13(2), $T_{c(onset)} = 100$ K). Another explanation for the lower transition temperature for BVS = 2.084 could be the presence of Y at the Ca site. The three-valent ion might draw the in-plane oxygen toward Y, which would decrease the valence of Cu as well as make the layer puckering more pronounced. Wu *et al.* (31) also examined $(Tl_{0.7}Hg_{0.3})_2Ba_2(Y_{0.8}Ca_{0.2})Cu_2O_{8+\delta}$, and they determined the effect of postannealing in Ar. With prolonged annealing, T_c decreased until the material was no longer superconducting. Examining the fractional coordinates, it was possible to see that the apical oxygen came marginally closer to Cu while the in-plane oxygen moved away, since the *a* axis cell parameter increased significantly. Therefore, one could presume that the BVS decreased as the superconductivity disappeared. Again, if the as-prepared and the reduced $(Tl_{0.7}Hg_{0.3})_2Ba_2(Y_{0.8}Ca_{0.2})Cu_2O_{8+\delta}$ could be added to the BVS–$T_{c(onset)}$ comparison, there should be a maximum around the 100 K sample, after which $T_{c(onset)}$ ought to decrease, together with a lowering of the Cu oxidation state.

It should be noted that the optimum hole concentrations (n_{opt} [holes/(Cu–O layer × unit cell)]) are similar for three different compounds: $(Tl,Hg)_2(Ba,Sr)_2(Sr,Ca)_1Cu_2O_{8-\delta}$ (Tl/Hg ~ 3, $n_{opt} = 0.13(2)$), $Hg_1Ba_2Ca_1Cu_2O_{6+\delta}$ ($n_{opt} = 0.11(1)$) (2), and $Bi_2Sr_2Ca_1Cu_2O_{8-\delta}$ ($n_{(T_c=85\,K)} = 0.15(3)$) (32), which might suggest a common feature for the bilayered cuprate superconductors, i.e., those containing two Cu–O layers per unit cell. Unfortunately, the well-known $Y_1Ba_2Cu_3O_{7-\delta}$ deviates from the mentioned property, as it has a significantly higher hole concentration. Worth mentioning is that a monolayered superconductor (Hg-1201) (33) also has its highest T_c for a hole concentration between 0.14 and 0.20, close to that of the compounds discussed previously.

CONCLUSIONS

A series of samples with the general composition $(Tl,Hg)_2(Ba,Sr)_2(Sr,Ca)_1Cu_2O_{8-\delta}$ (Tl/Hg ~ 3) were phase-pure enough to be analyzed by Rietveld calculations. Some correlations could be found between structural properties and the superconducting transition temperatures. The variation in diamagnetic transition temperatures was confirmed by resistivity measurements on a few of the polycrystalline bulk samples.

Changes in cell parameters (*a* and *c*), some interatomic distances, and the BVS for Cu correlated with the tendency of $T_{c(onset)}$. The larger of the two alkaline-earth metal sites, containing (Ba,Sr), seems to have a great influence on structure and properties. As the Ba/Sr ratio increases, several bonds are extended at the same time the occupancy of the oxygen site within the charge reservoir (O3) is suppressed. This is concluded from the changes in Cu valence, which is assumed to be closely connected with the hole concentration. The optimum hole concentration was approximately 0.13/superconducting layer in a unit cell. This result agrees well with previously published results for Hg-based (2) and Bi-based (32) superconductors, assuming that the phases in question are comparable. Future investigations will be performed at temperatures closer to the T_c to see if correlations between structure and properties will become more pronounced.

ACKNOWLEDGMENTS

We are grateful for economic support from The Swedish Natural Science Research Council (NFR). Gratitude is also extended to Jekabs Grins for invaluable interpretations of some diffraction data. M.V. also thanks Ivan Bozovic for helpful discussions.

REFERENCES

1. N. Nücker, J. Fink, J. C. Fuggle, P. J. Durham, and W. M. Temmerman, *Phys. Rev. B* **37,** 5158–5163 (1988).
2. M. Marezio, J.-J. Capponi, P.-G. Radaelli, P. P. Edwards, A. R. Armstrong, and W. I. F. David, *Eur. J. Solid State Inorg. Chem.* **t. 31,** 843–854 (1994).
3. G. F. Sun, K. W. Wong, B. R. Xu, Y. Xin, and D. F. Lu, *Phys. Lett. A* **192,** 122 (1994).
4. K. Isawa, A. Tokiwa-Yamamoto, M. Itoh, S. Adachi, and H. Yamauchi, *Physica C* **217,** 11 (1993).
5. H. Higuma, S. Miyashita, and M. Wakata, *Physica C* **291,** 302–308 (1997).
6. M. A. Alario-.Franco, C. Chaillout, J. J. Capponi, J.-L. Tholence, and B. Souletie, *Physica C* **222,** 52–56 (1994).
7. M. A. Subramanian, G. H. Kwei, J. B. Parise, J. A. Goldstone, and R. B. Von Dreele, *Physica C* **166,** 19–24 (1990).
8. F. Letouzé, S. Peluau, C. Michel, A. Maignan, C. Martin, M. Hervieu, and B. Raveau, *J. Mater. Chem.* **4**(8), 1353–1355 (1994).

9. T. Ohta, F. Izumi, A. Tokiwa-Yamamoto, K. Tanabe, and A. W. Hewat, *Physica C* **281,** 228–236 (1997).
10. A. Maignan, M. Hervieu, C. Martin, C. Michel, and B. Raveau, *Physica C* **232,** 15–21 (1994).
11. G. Nilsson and I. Bryntse, *J. All. Comp.* **259,** 200–207 (1997).
12. N. R. Khasanova, I. Bryntse, and E. V. Antipov, *Physica C* **247,** 197–205 (1995).
13. M. Hervieu, G. Van Tendeloo, A. Maignan, C. Michel, F. Goutenoire, and B. Raveau, *Physica C* **216,** 264 (1993).
14. M. Valldor, I. Bryntse, and A. Morawski, *Physica C* **314,** 27–35 (1999).
15. K. Knízek, S. Malo, C. Michel, A. Maignan, E. Pollert, and B. Raveau, *Eur. J. Solid State Inorg. Chem.* **t.34,** 1063–1074 (1997).
16. C. Ström, L.-G. Johansson, S.-G. Eriksson, and L. Börjesson, *Physica C* **185–189,** 623–624 (1991).
17. M. Valldor, and I. Bryntse, *J. Low Temp. Phys.* **117,** 867–871 (1999).
18. T. Roisnel and J. Rodríguez-Carvajal, "Fullprof 98 V. 0.2." Laboratoire Léon Brillouin (CEA-CNRS), 91191 Gif-sur-Yvette Cedex, France, 1998.
19. I. Bryntse, *Physica C* **226,** 184–187 (1994).
20. Y. Shimakawa, Y. Kubo, T. Manako, Y. Nakabayaski, and H. Igarashi, *Physica C* **156,** 97–102 (1988).
21. M. Hjorth and J. Hyldtoft, *Acta Chem. Scand.* **44,** 516–518 (1990).
22. K. Wong-Ng, K. L. Davis, and R. S. Roth, *J. Am. Ceram. Soc.* **71,** C64–C67 (1988).
23. M. T. Weller and D. R. Lines, *J. Chem. Soc. Chem. Commun.* 484–485 (1989).
24. I. D. Brown and D. Altermatt, *Acta Crystallogr. B* **41,** 244–247 (1985).
25. T. Stephen, C. Hormillosa, and S. Healy, "Bond Valence Calculations V. 2.00." Institute For Material Research, McMaster University, Hamilton, Ontario, Canada, 1993.
26. J.-F. Bérar and P. Lelann, *J. Appl. Crystallogr.* **24,** 1–5 (1991).
27. H. Romberg, N. Nücker, M. Alexander, J. Fink, D. Hahn, T. Zetterer, H.H. Otto, and K.F. Renk, *Phys. Rev. B* **41,** 2609–2611 (1990).
28. J. P. Attfield, A. L. Kharlanov, and J. A. McAllister, *Nature* **394,** 157–159 (1998).
29. C. W. Chu, L. Gao, F. Chen, Z.J. Huang, R.L. Meng, and Y.Y. Xue, *Nature* **365,** 323–325 (1993).
30. A. Maignan, C. Martin, C. Michel, M. Hervieu, and B. Raveau, *Chem. Mater.* **7,** 1207–1213 (1995).
31. X.-J. Wu, A. Tokiwa-Yamamoto, T. Tatsuki, S. Adachi, and K. Tanabe, *Physica C* **314,** 219–227 (1999).
32. J. M. Tarascon, W. R. McKinnon, P. Barboux, D. M. Hwang, B. G. Bagley, L. H. Greene, G. W. Hull, Y. LePage, N. Stoffel, and M. Giroud, *Phys. Rev. B* **38,** 8885–8892 (1988).
33. J. D. Jorgensen, O. Chmaissem, J. L. Wagner, W. R. Jensen, B. Dabrowski, D. G. Hinks, and J. F. Mitchell, *Physica C* **282–287,** 97–100 (1997).